"Comparison of diffusion models in the modelling of a catalytic membrane fixed bed reactor coupling dehydrogenation of ethylbenzene with hydrogenation of nitrobenzene."

by *Abo-Ghander, N.S.; Logist, Filip; Grace, J.R.; Van Impe, J.; Elnashaie, S.S.E.H. and Lim, C.J.*

N.S. Abo-Ghander, F. Logist, J.R. Grace, J.F.M. Van Impe, S.S.E.H. Elnashaie and C.J. Lim 2012. Comparison of diffusion models in the modelling of a catalytic membrane fixed bed reactor coupling dehydrogenation of ethylbenzene with hydrogenation of nitrobenzene, Computers and Chemical Engineering 38: 11-23.

Comparison of Diffusion Models in the Modelling of a Catalytic Membrane Fixed Bed Reactor Coupling Dehydrogenation of Ethylbenzene with Hydrogenation of Nitrobenzene

Nabeel S. Abo-Ghander (1), Filip Logist (2), John R. Grace* (1), Jan F.M. Van Impe(2), Said S.E.H. Elnashaie(1), and C. Jim Lim(1)

(1) Chemical and Biochemical Engineering Department, University of British Columbia, Vancouver, Canada V6T 1Z3
(2) BioTeC and OPTEC, Department of Chemical Engineering, Katholieke Universiteit Leuven, W. de Croylaan 46, B-3001 Leuven, Belgium

---

* Corresponding author. Fax: +1-604-822-6003.
E-mail address: John R. Grace (jgrace@chbe.ubc.ca).

Journal homepage: http://www.sciencedirect.com/science/journal/00981354
Original file available at: http://dx.doi.org/10.1016/j.compchemeng.2011.10.007

Abstract:

Coupling of dehydrogenation of ethylbezene with hydrogenation of nitrobenzene in a catalytic membrane reactor can lead to a significant improvement in the conversion of ethylbenzene and production of styrene. In this work, the homogeneous reactor model for a concurrent flow configuration is compared to two heterogeneous models based on the Fickian diffusion model and the dusty gas model for both isothermal and non-isothermal pellets. It is observed that both heterogeneous models predict a significant drop in yield and conversion compared to the homogeneous model, indicating the importance of heterogeneity. This drop is generally less severe for the dusty gas model than for the Fickian diffusion model. The assumption of isothermality causes larger deviations than the assumption of Fickian diffusion. The deviations in the predictions of the homogenous model and the heterogeneous models from those of the dusty gas model for non-isothermal pellets are ~6% and ~11%, respectively.

Keywords: membrane reactor, dehydrogenation, hydrogenation, homogeneous model, heterogeneous model, dusty gas model, Fickian diffusion model

1 Introduction

Membrane reactors can significantly improve the production rates of thermodynamically-limited reactions. Hydrogen-selective membranes permit hydrogen produced by reactions to escape under the influence of the difference in the hydrogen partial pressures to the permeate side where an inert gas such as nitrogen can be used to purge hydrogen. This type of reactor is promising for thermodynamically limited reactions such as steam reforming. A number of studies have reported that when steam reforming is operated in membrane reactors, hydrogen yields can exceed those in simple fixed bed reactors (Balasubramanian et al., 1999; Chen and Elnashaie, 2005; Chen et al., 2003; Itoh et al., 2003; Rakib et al., 2008; Tiemersma et al., 2006; Uemiya et al., 1990).

Another type of reaction suffering from thermodynamic limitations is the one involving the production of olefins from inexpensive parafins via dehydrogenation. Shifting the equilibrium production rate of these thermodynamically-limited dehydrogenation reactions was the objective of a number of studies reported in the last decade. Several reactor configurations and models have stimulated these configurations. In general, the hydrogen membranes facilitate hydrogen transfer to the permeate side where it is collected by a sweep gas (Hermann et al., 1997; Itoh et al., 2003) or utilized as a reactant in complementary reactions (Abo-Ghander et al., 2008; Abdalla et al., 1997; Elnashaie et al., 2000; Itoh and Wu, 1997; Moustafa and Elnashaie, 2000).

Dehydrogenation of ethylbenzene to styrene and hydrogenation of nitrobenzene to aniline complement each other and constitute a synergistic pair of reactions to couple in a catalytic membrane fixed bed reactor (Abo-Ghander et al., 2008). Diffusion of hydrogen produced on the dehydrogenation side through hydrogen-selective membranes assists greatly in shifting forward the equilibrium conversion of ethylbenzene, while simultaneously improving the yield of styrene compared with fixed bed reactors without membranes. Combining the two reactions in this manner helps to significantly increase the production of styrene on the dehydrogenation side and to produce aniline as a second useful product on the hydrogenation side. Transferring the heat released from the

Journal homepage: http://www.sciencedirect.com/science/journal/00981354
Original file available at: http://dx.doi.org/10.1016/j.compchemeng.2011.10.007

hydrogenation side to the dehydrogenation side also helps to promote the forward dehydrogenation reaction of ethylbenzene, consequently enhancing the styrene yield (Abo-Ghander et al., 2008). In this configuration, it is possible to boost the styrene yield from ~40% in catalytic industrial reactors (Moustafa and Elnashaie, 2000) to ~98% in an optimized catalytic membrane reactor (Abo-Ghander et al., 2010a).

Abo-Ghander et al. (2010b) briefly assessed the effect of the intraphase transport by considering diffusion inside the catalyst pellets on both sides of the coupled membrane reactor. The Fickian diffusion model was used in which the reactants are assumed to diffuse through a stagnant bulk phase with the diffusivities of components in the reacting mixture along the radial direction inside the catalyst pellets evaluated by the well-known Wilke equation. The predictions of the heterogeneous model are significantly less than that of the homogeneous model, providing an indication of the importance of the intraparticle transport resistances.

In catalytic packed bed reactors, the components in reacting mixtures have to diffuse through tortuous complex networks of pores ranging from macropores to micropores to reach active sites, where they react. Hence, the selection of an appropriate diffusion model accounting for intraphase resistances is highly important when modeling these types of reactors. The Fickian diffusion model is considered to yield accurate predictions if the reacting component diffuses in a large excess of a second component and there is no appreciable change in the number of moles. In contrast, the dusty gas model is considered to be more general but also more complex. As the assumptions for Fickian diffusion may not always be met in the studied reactor (Elnashaie and Abashar, 1993; Elnashaie et al., 1993), the aim of this paper is not only to rigorously evaluate the effect of intraparticle diffusion, but also to compare the Fickian diffusion and the dusty gas model. Moreover, also the effect of isothermal versus non-isothermal catalyst pellets is studied.

Section 2 introduces the reactor configuration, while Section 3 describes the reactor models and focuses especially on the incorporation of intraphase resistances based on the

Fickian diffusion and the dusty gas model. Section 4 presents and compares the simulation results for all models. Finally, Section 5 summarizes the main conclusions.

2 Reactor Configuration

A conceptual schematic of the integrated reactor proposed by Abo-Ghander et al. (2008) appears in Fig. 1. The reactor is composed of two compartments provided by a shell containing a bundle of hydrogenation tubes. On the shell side, dehydrogenation of ethylbenzene takes place producing styrene and hydrogen. Five side reactions also occur, producing benzene, toluene, and light gases like ethylene, methane, carbon monoxide, and carbon dioxide. The stoichiometric equations on the shell side can be expressed as:

$$C_6H_5CH_2CH_3 \leftrightarrow C_6H_5CHCH_2 + H_2 \qquad \Delta H_{298} = 117.6\,\frac{kJ}{mole} \qquad (1)$$

$$C_6H_5CH_2CH_3 \rightarrow C_6H_6 + C_2H_4 \qquad \Delta H_{298} = 105.4\,\frac{kJ}{mole} \qquad (2)$$

$$C_6H_5CH_2CH_3 + H_2 \rightarrow C_6H_5CH_3 + CH_4 \qquad \Delta H_{298} = -54.6\,\frac{kJ}{mole} \qquad (3)$$

$$2H_2O + C_2H_4 \rightarrow 2CO + 4H_2 \qquad \Delta H_{298} = 210.2\,\frac{kJ}{mole} \qquad (4)$$

$$H_2O + CH_4 \rightarrow CO + 3H_2 \qquad \Delta H_{298} = 206.1\,\frac{kJ}{mole} \qquad (5)$$

$$H_2O + CO \rightarrow CO_2 + H_2 \qquad \Delta H_{298} = -41.2\,\frac{kJ}{mole} \qquad (6)$$

In industrial fixed bed reactors producing styrene, the temperature tends to drop along the reactor due to the endothermic nature of the main reaction if sufficient heat is not supplied. In the proposed membrane reactor, hydrogen produced on the shell side diffuses through a palladium hydrogen-selective-membranes to the tube side where it intermingles with a feed stream containing only nitrobenzene and steam. The membrane wall considered is made up of two layers: a layer of stainless steel of a thickness 0.0012 m, coated by a palladium layer of a thickness 20×10^{-6} m.

Inside the membrane tubes, cocurrently flowing nitrobenzene reacts with hydrogen to produce aniline as a second major useful product from the integrated membrane reactor.

$$C_6H_5NO_2 + 3H_2 \rightarrow C_6H_5NH_2 + 2H_2O \qquad \Delta H_{298} = -443.0\,\frac{kJ}{mole} \qquad (7)$$

This hydrogenation reaction is irreversible and highly exothermic. The heat generated by this reaction is transferred through the membrane layer and heats the reacting mixture on the dehydrogenation side.

The catalyst on the shell side is composed of iron oxide (Fe_2O_3) promoted by potassium carbonate (K_2CO_3) and chromium oxide (Cr_2O_3), whereas that on the tube side is a palladium catalyst supported on an α-alumina carrier. Tables 1 and 2 summarize the kinetics, frequency factors and activation energies (Amon et al., 1999; Elnashaie et al., 1993).

3 Reactor Model

The differential equations governing the behavior of different chemical species on both sides of the reactor, as well as the temperature profiles are derived considering two infinitesimal slices across which exchanges of moles and energy take place. The following assumptions are adopted.

1. Steady state operation.
2. Ideal gas behavior on both the shell and tube compartments.
3. Plug flow for the fixed beds on both the shell and tube sides.
4. Heterogeneous model, i.e. there are concentration and temperature gradients within the catalyst particles.
5. The flow rates on both sides are large enough to minimize external mass and heat transfer resistances. Only intraparticle diffusion is considered.
6. The reactor external wall is adiabatic.

Original file available at: http://dx.doi.org/10.1016/j.compchemeng.2011.10.007

7. Catalyst deactivation is neglected.
8. Pressure gradients along both compartments are estimated based on Ergun's equation.

Along the integrated membrane reactor, hydrogen diffuses from the dehydrogenation side to the hydrogenation side while heat is transferred from the hydrogenation to the dehydrogenation side. The reactor model equations and the rates of both hydrogen diffusion and heat transfer per unit length are given in Table 3.

3.1 Diffusion inside the catalyst pellets

Fixed bed reactors suffer from diffusion limitations resulting in temperature and concentration gradients between the bulk and surface of the catalysts (external mass and heat transfer), and between the surface of the catalyst pellets and the active sites inside the catalysts (intraparticle mass and heat transfer). Consequently, the concentration and temperature profiles between those phases are not flat anymore causing the homogeneous model predictions to be not always highly accurate (Elnashaie and Elshishini, 1993).

Operating the reactor at high flow rates can greatly enhance the external mass and heat transfer coefficients, consequently minimizing the effect of external mass and heat transfer resistances. The effect of the intraparticle heat and mass transfer resistances, however, cannot be reduced due to the significant size of the catalyst pellets, ranging from 6 to 14 mm. As a result, neglecting the effect of the intraparticle resistance when modeling fixed bed reactors may result in a considerable discrepancy between the model predictions and reality (Elnashaie and Alhabdan, 1989).

Two diffusion models are commonly used to account for the intraparticle mass transfer resistance, namely the Fickian diffusion model and the dusty gas model. The Fickian diffusion model is in general less accurate, but is the most widely used due to its simplicity (Veldsink et al., 1995). It can be easily derived from the dusty gas model after neglecting the effect of the ratio of component molar fluxes. This approximation reduces the accuracy of the Fickian diffusion model especially in reactive systems subject to changes in molar flow rates.

The dusty gas model is more rigorous than the Fickian diffusion model. It is considered to be the most general model for treating diffusion in non-ideal systems and for systems influenced by external force fields (Krishna and Wesselingh, 1997). It can also be used to model diffusion in macro- and micro-porous catalysts (Veldsink et al., 1995), adsorbents (Krishna, 1990) and membranes (Beuscher and Gooding, 1999). The porous medium is treated in the dusty gas model as composed of giant fixed molecules uniformly distributed in space, and referred to as dust and treated as one component of the gas mixture. The model has been used widely in the modeling of reactive systems involving gases.

Both models have been used by a number of researchers to predict the diffusion inside catalysts. For example, the Fickian diffusion model was used by Wang et al., 2001 to model the diffusion inside non-isothermal catalysts in Fischer-Tropsch synthesis. Diffusion inside the catalyst pellets has been studied for steam reforming of methane based on the Fickian diffusion model, the dusty gas model and another simplified model derived from the dusty gas model. Because the reaction is characterized by high diffusion limitations, a deviation in the predictions of the Fickian diffusion model and a (simplified) dusty gas model was observed at high steam-to-methane ratios. The dusty gas model is recommended for rigorous predictions of the influence of intraparticle diffusion (Abashar and Elnashaie, 1993; Elnashaie et al., 1992; Elnashaie and Abashar, 1993; Soliman et al., 1988).

3.2 Diffusion models for the catalyst pellets

The molar and energy fluxes inside the catalyst pellets are estimated based on the following assumptions:

1. Steady-state molar and energy flow.
2. Particles are spherical and their porous structure is isentropic.
3. Ideal gas law.
4. Concentration and temperature profiles within the catalyst particles are spherically symmetrical.
5. External mass and heat transfer resistances are negligible due to the high gas flow rates.
6. Negligible viscous flow inside the catalyst particles; the pellets are isobaric.
7. Convective diffusion is neglected, only ordinary molecular and Knudsen diffusion are significant for gas motion within the solid particles.
8. Convective energy transfer is negligible.
9. Thermal conductivities of the catalyst pellets are constant on both sides of the reactor.

To obtain the dusty gas model describing the diffusion inside the catalyst pellets, the molar and energy fluxes around a small shell inside the catalyst pellet on the dehydrogenation side are considered as shown in Figure 2. Applying the balance equations around the shell with no accumulation leads to:

$$\left(4\pi y^2 N_i\right)\Big|_y - \left(4\pi y^2 N_i\right)\Big|_{y+\Delta y} + \sum_{j=1}^{6} \sigma_{ij} r_j \rho \left(4\pi y^2 \Delta y\right) = 0 \qquad (16)$$

$$\left(4\pi y^2 q\right)\Big|_y - \left(4\pi y^2 q\right)\Big|_{y+\Delta y} + \sum_{j=1}^{6} \left[-\Delta H\left(T\right)\right] r_j \rho \left(4\pi y^2 \Delta y\right) = 0 \qquad (17)$$

When the shell thickness approaches zero, equations (16) and (17) become:

$$\frac{dN_i}{dy} + \frac{2}{y} N_i = \sum_{j=1}^{6} \sigma_{ij} r_j \rho \qquad (18)$$

$$\frac{dq}{dy}+\frac{2}{y}q=\sum_{j=1}^{6}\left[-\Delta H\left(T\right)\right]_{j}r_{j}\rho \tag{19}$$

Expressing the heat flux in equation (19) by Fourier's law leads to:

$$\frac{d^{2}T}{dy^{2}}+\frac{2}{y}\frac{dT}{dy}=\frac{1}{k_{e}}\sum_{j=1}^{6}\left[\Delta H\left(T\right)\right]_{j}r_{j}\rho \tag{20}$$

The molar flux in equation (18) is related to the component mole fractions by the Stefan-Maxwell diffusion equation. When the pressure drop is neglected, this can be written (Veldsink et al., 1995) as:

$$\frac{P}{RT}\nabla x_{i}=\sum_{\substack{j=1\\ j=i}}^{10}\frac{x_{i}N_{j}-x_{j}N_{i}}{D_{ij}^{e}}-\frac{N_{i}}{D_{ik}^{e}} \tag{21}$$

For a one-dimensional problem in spherical coordinates, equation (21) becomes:

$$\frac{P}{RT}\frac{dx_{i}}{dy}=\sum_{\substack{j=1\\ j\neq i}}^{10}\frac{x_{i}N_{j}-x_{j}N_{i}}{D_{ij}^{e}}-\frac{N_{i}}{D_{ik}^{e}} \tag{22}$$

Equations analogous to equations (18), (20) and (22) may be written to describe the diffusion inside the catalyst pellets on the hydrogenation side:

$$\frac{dN_{i}'}{dy'}+\frac{2}{y'}N_{i}'=\sigma_{i}'r'\rho' \tag{23}$$

$$\frac{d^{2}T'}{dy'^{2}}+\frac{2}{y'}\frac{dT'}{dy'}=\frac{\left[\Delta H\left(T\right)\right]'r'\rho'}{k_{e}'} \tag{24}$$

$$\frac{P'}{RT'}\frac{dx'_i}{dy'}=\sum_{\substack{j=1\\ j\neq i}}^{4}\frac{x'_iN'_j-x'_jN'_i}{D'^{e}_{ij}}-\frac{N'_i}{D'^{e}_{ik}} \tag{25}$$

Alternatively, the diffusion inside the catalyst pellets can be described by the Fickian diffusion model. For multicomponent systems, Fick's law is expressed (Froment and Bischoff, 1990; Elnashaie and Elshishini, 1993) as:

$$N_i=-D_{ie}\frac{dC}{dy} \tag{26}$$

where the diffusivity of component i is expressed (Abashar and Elnashaie, 1993; Elnashaie et al., 1992; Elnashaie and Elshishini, 1993) as:

$$\frac{1}{D_{ie}}=\frac{1}{D^{e}_{im}}+\frac{1}{D^{e}_{ik}} \tag{27}$$

The diffusivity of component i in the mixture is calculated using the Wilke equation:

$$\frac{1-x_i}{D_{im}}=\sum_{\substack{j=1\\ j\neq i}}^{10}\frac{x_j}{D_{ij}} \qquad 1\le i\le 10 \tag{28}$$

where effective diffusivities are defined (Froment and Bischoff, 1990; Elnashaie and Elshishini, 1993) as:

$$D^{e}_{im}=\frac{\varepsilon}{\tau}D_{im} \tag{29}$$

Inserting equation (27) into (18) gives the Fickian diffusion model on the dehydrogenation side (Abo-Ghander et al., 2010b) as:

$$\frac{d^2C_i}{dy^2}+\frac{2}{y}\frac{dC_i}{dy}=-\frac{1}{D_{ie}}\sum_{j=1}^{6}\sigma_{ij}r_j\rho \tag{30}$$

Similarly, on the hydrogenation side, the Fickian diffusion model equation is written as:

$$\frac{d^2C_i'}{dy'^2}+\frac{2}{y'}\frac{dC_i'}{dy'}=-\frac{\sigma_i' r'\rho'}{D_{ie}'} \qquad (31)$$

In the above set of equations, the dusty gas model requires solution of the coupled equations (18), (20) and (22) on the dehydrogenation side and (23), (24) and (25) on the hydrogenation side. On the other hand, the Fickian diffusion model is given by the coupled equations (20) and (30) on the dehydrogenation side and (24) and (31) on the hydrogenation side. Each pair of these equations forms a set of split boundary value problems describing the molar and energy fluxes inside the catalyst on both sides of the reactor. These pairs must be solved at each axial position along the reactor to evaluate the volume-averaged reaction rates, as well as the volume-averaged heat of reactions. The corresponding boundary conditions for the dusty gas model are:

- on the dehydrogenation side:

Centre of the catalyst pellets:

$$y=0\Rightarrow\begin{cases}N_i=0\\ \dfrac{dT}{dy}=0\end{cases} \qquad (32)$$

Surface of the catalyst pellets:

$$y=R_p\Rightarrow\begin{cases}x_i=x_{is}\\ T=T_s\end{cases} \qquad (33)$$

- on the hydrogenation side:

Centre of the catalyst pellets:

$$y'=0\Rightarrow\begin{cases}N_i'=0\\ \dfrac{dT'}{dy'}=0\end{cases} \qquad (34)$$

Journal homepage: http://www.sciencedirect.com/science/journal/00981354
Original file available at: http://dx.doi.org/10.1016/j.compchemeng.2011.10.007

Surface of the catalyst pellets: $$y' = R'_p \Rightarrow \begin{cases} x'_i = x'_{is} \\ T' = T'_s \end{cases} \qquad (35)$$

For the Fickian diffusion mode, the boundary conditions:

- on the dehydrogenation side:

Centre of the catalyst pellets: $$y = 0 \Rightarrow \begin{cases} \dfrac{dC_i}{dy} = 0 \\ \dfrac{dT}{dy} = 0 \end{cases} \qquad (36)$$

Surface of the catalyst pellets: $$y = R_p \Rightarrow \begin{cases} C_i = C_{is} \\ T = T_s \end{cases} \qquad (37)$$

- on the hydrogenation side:

Centre of the catalyst pellets: $$y' = 0 \Rightarrow \begin{cases} \dfrac{dC'_i}{dy} = 0 = 0 \\ \dfrac{dT'}{dy'} = 0 \end{cases} \qquad (38)$$

Surface of the catalyst pellets: $$y' = R'_p \Rightarrow \begin{cases} C'_i = C'_{is} \\ T' = T'_s \end{cases} \qquad (39)$$

Numerical solution of the dusty gas and Fickian diffusion on the hydrogenation side of the reactor leads to the evaluation of the volume-averaged reaction rates and the volume averaged heat released or absorbed due to reactions. These values can be related to the bulk concentrations and temperatures through effectiveness factors, defined as the ratio of the reaction rate with pore resistance to the reaction rate which would prevail if the concentrations and temperature throughout the particles were equal to those at the surface.

$$\eta_j = \frac{\int_0^{R_p} r_j \rho \left(4\pi y^2\right) dy}{r_j \rho \left(\frac{4}{3}\pi R_p^3\right)} \tag{40}$$

Introducing the dimensionless catalyst radius ($\omega = \frac{y}{R_p}$) into equation (40) leads to:

$$\eta_j r_j \left(T_s, C_{is}\right) = 3\int_0^{1.0} r_j\, \omega^2 d\omega \tag{41}$$

where:

$1 \le j \le 6$ for the dehydrogenation side

$j = 1$ for the hydrogenation side

For non-isothermal catalyst pellets, the volume-averaged heat of reaction is defined as:

$$\eta_j [\Delta H\left(T_s\right)] r_j \left(C_{is}, T_s\right) = 3\int_0^{1.0} [\Delta H\left(T\right)]_j\, r_j \left(C_i, T\right) \omega^2 d\omega \tag{42}$$

with j as for equation (41). Integral terms in equations (41) and (42) were evaluated numerically by the trapezoidal rule. Equations (41) and (42) represent the actual reaction rates and actual heat of reactions, and they are used to update the reactor model, equations (8) to (13) in Table 3.

The conversion of ethylbenzene on the dehydrogenation side, the conversion of nitrobenzene on the hydrogenation side and component yields on the dehydrogenation side along the reactor are defined as:

$$\text{Conversion} = \begin{cases} X_{EB} = \dfrac{n_{EBo} - n_{EB}}{n_{EBo}} & \text{Dehydrogenation Side} \\ X_{NB} = \dfrac{n_{NBo} - n_{NB}}{n_{NBo}} & \text{Hydrogenation Side} \end{cases} \tag{43}$$

$$\text{Yield} = \begin{cases} Y_{ST} = \dfrac{n_{ST} - n_{STo}}{n_{EBo}} \\ Y_{BZ} = \dfrac{n_{BZ} - n_{BZo}}{n_{EBo}} \\ Y_{TO} = \dfrac{n_{TO} - n_{TOo}}{n_{EBo}} \end{cases} \tag{44}$$

Mean square and absolute deviations from the best model predictions are defined for the styrene yield and nitrobenzene conversion as:

$$\text{Mean square deviation} = \begin{cases} \sqrt{\dfrac{1}{N_p}\sum_{i=1}^{N_p}(Y_{ST}^i - \tilde{Y}_{ST}^i)^2} & \text{for styrene yield} \\ \sqrt{\dfrac{1}{N_p}\sum_{i=1}^{N_p}(X_{NB}^i - \tilde{X}_{NB}^i)^2} & \text{for nitrobenzene conversion} \end{cases} \tag{45}$$

$$\text{Mean absolute deviation} = \begin{cases} \dfrac{1}{N_p}\sum_{i=1}^{N_p}\left|Y_{ST}^i - \tilde{Y}_{ST}^i\right| & \text{for styrene yield} \\ \dfrac{1}{N_p}\sum_{i=1}^{N_p}\left|X_{NB}^i - \tilde{X}_{NB}^i\right| & \text{for nitrobenzene conversion} \end{cases} \tag{46}$$

The sequence of computations which successfully couples the diffusion models with the reactor model is depicted in Figure 3. At the inlet of the reactor, the feed conditions, i.e. feed molar flow rates, inlet temperatures and inlet pressures, provide boundary conditions for the catalyst equations (33), (35), (37) and (39). The dusty gas model and the Fickian diffusion model equations on both sides of the reactor are solved numerically using the Matlab® (The MathWorks, Natick) routine `bvp4c` with a relative tolerance of 1×10^{-4} in order to retrieve the molar flux, mole fraction and temperature profiles inside the catalyst pellets. Those profiles are used to calculate the volume-averaged reaction rates and volume-averaged heat of reactions by numerically evaluating the integrals in equations (41) and (42). The reactor model equations are then integrated one step forward and this procedure continues until the whole length is covered. For this integration the Matlab® routine `ode15s` is employed with relative and absolute tolerances of 1×10^{-8}.

4 Results and Discussion

The model of the catalytic membrane reactor was solved for the operating conditions in Table 4. The molar flow rate and feed pressure were set to match the industrial values given by Moustafa and Elnashaie (2000). The feed temperature on the dehydrogenation side was adjusted to ensure the sustainability of the membrane, i.e. the local temperature of the membrane must never exceed 923 K. On the hydrogenation side, the total molar feed rate is 17 mole/s composed of only nitrobenzene and steam. The feed temperature on the hydrogenation side is chosen to ensure that heat always flows from the hydrogenation to the dehydrogenation side. Three models, i.e. the homogeneous and heterogeneous based on the Fickian diffusion and the dusty gas model, are evaluated. In addition, the influence of isothermal versus non-isothermal catalyst pellets is assessed for both heterogeneous models.

4.1 Conversion of ethylbenzene and nitrobenzene

The conversion of ethylbenzene on the dehydrogenation side and nitrobenzene on the hydrogenation side versus the dimensionless distance along the membrane reactor are plotted in Figures 4a and 4b for the homogenous model and heterogeneous models based on Fickian diffusion and the dusty gas model, for isothermal and non-isothermal catalyst particles. All three models predict monotonic increases on the dehydrogenation side as shown in Figure 4a. The predictions of the three models, however, diverge due to the different methods of assessing the intraphase transport resistances. For example, the overall ethylbenzene conversion is predicted to be ~88% by the homogeneous model,

~78% and ~71% by the heterogeneous reactor model based on Fickian diffusion for isothermal and non-isothermal catalyst pellets, and ~79% and ~75% according to the heterogeneous reactor model incorporating the dusty gas model for isothermal and non-isothermal catalyst pellets, respectively.

On the hydrogenation side, the nitrobenzene conversion is plotted versus the axial dimensionless distance in Figure 4b. The overall conversion is predicted to be ~68% by the homogeneous model compared with ~59% and ~52% by the heterogeneous reactor model with Fickian diffusion for isothermal and non-isothermal catalyst pellets, and ~61% and ~57% according to the heterogeneous reactor model in conjunction with the dusty gas model for isothermal and non-isothermal catalyst pellets, respectively.

4.2 Yield of styrene, benzene, and toluene on dehydrogenation side

The yields of styrene, benzene, and toluene on the dehydrogenation side are plotted against the dimensionless axial distance based on all three reactor models in Figures 5a, 5b, and 5c, respectively. The yields of all three components from the reactor models are predicted to increase monotonically along the reactors. Predictions, on the other hand, differ from one model to another due to the alternative intraparticle resistances. For example, the homogenous model predicts an overall styrene yield of ~82%, a benzene yield of ~5.0%, and a toluene yield of ~1.0%, whereas the heterogeneous reactor model with Fickian diffusion predicts respective overall yields of ~73%, ~4.4% and ~0.9% for isothermal pellets and a styrene yield of ~68%, a benzene yield of ~3.0%, and a toluene yield of ~0.6% for non-isothermal pellets. The heterogeneous reactor model based on the dusty gas model predicts an overall styrene yield of ~73%, a benzene yield of ~4.6%, and a toluene yield of ~0.8% for isothermal pellets and respective overall yields of ~69%, ~4.4% and ~0.9% for non-isothermal pellets.

4.3 Hydrogen molar flow rates on dehydrogenation and hydrogenation sides

Predicted hydrogen molar flow rates on both sides of the reactor are plotted in Figures 6a, and 6b. On the dehydrogenation side, the hydrogen molar flow rate is predicted to increase linearly in the first portion of the membrane reactor as indicated in Figure 6a due to the significant net production of hydrogen. However, this is then balanced by the hydrogen diffusion through the membrane, causing the molar flow rate of hydrogen to become almost constant on the dehydrogenation side. The difference in predicting hydrogen molar flow rates between the homogenous reactor model and the heterogeneous model with Fickian diffusion for non-isothermal pellets is ~0.4 mole/s, whereas it is ~0.2 mole/s for the heterogeneous reactor model based on the dusty gas model for non-isothermal pellets.

On the hydrogenation side, the hydrogen molar flow rate is predicted to increase along the membrane reactor by all three reactor models, due to the significant hydrogen diffusion rate compared to its consumption rate. The heterogeneous reactor model based on Fickian diffusion for the isothermal pellet predicts a higher hydrogen flow near the entrance on the hydrogenation side than the homogenous model. The heterogeneous reactor model based on the dusty gas model for the non-isothermal pellets predicts a hydrogen flow similar to that predicted by the homogeneous model, whereas the other models all predict smaller hydrogen flow rates.

4.4 Temperature profiles along both sides of the coupled reactor

Predicted temperature profiles along the dehydrogenation side are plotted in Figure 7a for the homogeneous model, the heterogeneous model with the Fickian diffusion and the dusty gas model for the isothermal and the non-isothermal cases. In all five cases, the temperature is predicted to decrease at the entrance of the reactor due to the net endothermicity on the dehydrogenation side until a minimum is reached where the heat absorbed by reactions is balanced by that transferred from the hydrogenation side. Beyond this point, the temperature increases monotonically until the outlet of the reactor.

The point of balance occurs at a fractional length of ~0.2, but at different temperatures. The lowest temperature at which the point of balance occurs is predicted by the homogeneous model, while the highest is predicted by the heterogeneous reactor model with Fickian diffusion for non-isothermal pellets. The heterogeneous dusty gas model predicts intermediate values for both isothermal and non-isothermal pellets.

As shown in Figure 7b, the temperature on the hydrogenation side is predicted to increase along the reactor due to the high heat release from the hydrogenation reaction. Only the homogenous model predicts a clear point of balance. The temperatures predicted by the heterogeneous models become almost constant until the end of the reactor after a monotonic increase. The heterogeneous reactor model based on the dusty gas model gives intermediate temperature profiles for both isothermal and non-isothermal pellets compared to both the homogeneous reactor model and the heterogeneous model with Fickian diffusion.

4.5 Predictions of Styrene Yields and Nitrobenzene Conversions in the Coupled Reactor by the various Models

Previously, optimal trade-off curves for conflicting conversion and yield objectives were determined based on the homogeneous reactor model in Abo-Ghander et al. (2010a) using multi-objective approaches similar to those ones employed by Logist et al. (2009). The calculated optimal operating and design parameters for the coupled reactor are summarized in Table 5 for three cases: (i) focus on the production of only styrene, case A, (ii) equal focus on styrene and aniline as products, case B and (iii) focus on the production of only aniline, case C. The coupled reactor is simulated for these three cases using the heterogeneous reactor model based on dusty gas diffusion, listing the yield of styrene and the conversion of nitrobenzene in Table 5. The predicted styrene yields and nitrobenzene conversions differ significantly indicating the importance of intraparticle transport resistances and the sensitivity to the diffusion model inside the catalyst pellets. When Fickian diffusion is used to describe the intraparticle diffusion, the predicted styrene yields and nitrobenzene conversions are reduced more than when the dusty gas model is utilized. The homogeneous reactor model predicts higher styrene yields and nitrobenzene conversions because the effect of the intraparticle resistance is neglected while the Fickian diffusion model underestimates both the styrene yields and nitrobenzene conversions because it can be strictly applied for dilute systems and not for multicomponent ones. It cannot also account for the change of moles as dusty gas model does in reactive systems. All the previously mentioned reasons result in making the Fickian diffusion model only an approximating tool for complex reactive systems but not a well predicting one.

The deviations of the homogeneous model, the heterogeneous model with Fickian diffusion for isothermal and non-isothermal catalyst pellet cases and the heterogeneous model with dusty gas for the isothermal catalyst pellet case from the heterogeneous model with dusty gas for the non-isothermal catalyst pellet case are given in Table 6 for the base case operating conditions listed in Table 4 and the three optimization cases of Table 5. The prediction of the heterogeneous dusty gas model for the non-isothermal catalyst pellets is taken as the most accurate and sophisticated predictive model. The predictions of the styrene yield and nitrobenzene conversion by all other models are evaluated along the reactor with a dimensionless spacing of 0.1. Deviations are evaluated based on both the mean square deviation and mean absolute deviation. The highest deviation is observed for the homogenous reactor model, while the lowest is for the heterogeneous model with Fickian diffusion for the non-isothermal catalyst pellet case. The predictions of all other models are intermediate between these two models. The assumption of isothermality causes greater deviations than the Fickian diffusion simplification for all investigated cases. Moreover, even the worst heterogeneous model yields in all cases predictions within 6% of the most accurate model, compared to deviations of up to ~11% for the homogeneous model.

5 Conclusion

A catalytic membrane fixed bed reactor coupling the dehydrogenation of ethylbenzene with the hydrogenation of nitrobenzene is modeled in three ways: via a previously employed homogeneous model and two heterogeneous models one employing the Fickian diffusion and the other dusty gas model to describe the intraparticle transport. In these last two, both isothermal and non-isothermal catalyst pellets are considered. The homogeneous model overestimates both the yield of styrene on the dehydrogenation side and the conversion of nitrobenzene on the hydrogenation side, while the heterogeneous Fickian diffusion model under-predicts these quantities. The heterogeneous dusty gas diffusion model is more rigorous than the heterogeneous Fickian diffusion model, and it generally results in predictions intermediate between the homogenous and heterogeneous Fickian models. When all three models are compared with the heterogeneous reactor model with the dusty gas diffusion model for non-isothermal pellets, the highest deviation is observed for the homogeneous reactor model, while the lowest is provided by the heterogeneous reactor model with Fickian diffusion for non-isothermal catalyst pellets. However, even the worst of the heterogeneous models yields predictions within 6% of the most accurate model, while the deviations are up to ~11% for the homogeneous model.

Acknowledgement

The authors are very grateful to the Saudi Arabian government and to King Fahd University of Petroleum & Minerals (KFUPM) for sponsoring the studies of N. Abo-Ghander at the University of British Columbia. Work of F. Logist and J.F.M. Van Impe is supported in part by Projects OT/09/025/TBA, OPTEC (Center-of-Excellence Optimization in Engineering) EF/05/006 and SCORES4CHEM KP/09/005 of the Katholieke Universiteit Leuven, and by the Belgian Program on Interuniversity Poles of Attraction, initiated by the Belgian Federal Science Policy Office. J.F.M. Van Impe holds the Safety Engineering chair sponsored by the Belgian Chemistry and Life Sciences Federation Essenscia.

Notation

a_i	constant, 1 for hydrogen, 0 otherwise, [-].
A_{cs}, A'_{cs}	cross-sectional area of shell and tube sides, [m^2].

Cp_i, Cp'_i	heat capacity of component i on shell and tube sides, [J/mole/K].
C_i, C'_i	concentration of i inside catalyst pellets on shell and tube sides, [mole/m^3].
D	area-equivalent diameter on shell side, [m].
D_{ij}, D'_{ij}	binary diffusivity of i into j on shell and tube sides, [m^2/s].
D_{im}	diffusivity of component i into the mixture on shell side, [m^2/s].
D_{ik}, D'_{ik}	Knudsen diffusivity of i on shell and tube sides, [m^2/s].
D^e_{ij}, D'^e_{ij}	effective binary diffusivity of i into j on shell and tube sides j, [m^2/s].
D^e_{im}	effective component i into mixture on shell side, [m^2/s].
D^e_{ik}, D'^e_{ik}	effective Knudsen diffusivity of i on shell and tube sides, [m^2/s].
D^e_{ie}, D'^e_{ie}	mean diffusivity of i on shell and tube sides, [m^2/s].
D_p, D'_p	diameter of catalyst particles on shell and tube sides, [m].
D_t	diameter of tube, [m].
E_j, E'	activation energy of reaction j on shell side and hydrogenation reaction on tube side, [J/mole/K].
H_i, H'_i	enthalpy of component i on shell and tube sides, [J/mole].
k, k′	thermal conductivities of catalyst of shell and tube sides, [Jm/s].
k_{io}	reaction i pre-exponential factor, [mole/K^m/kg cat/s/bar^n], (for k_1 and k_2, m=0, n=1; for k_3 and k_5, m=0, n=2; for k_4, m=0, n=1.5; for k_6, m=3, n=3).
k_i	reaction i rate constant, [mole/K^m/kg cat/s/bar^n], (for k_1 and k_2, m=0, n=1; for k_3 and k_5, m=0, n=2; for k_4, m=0, n=1.5; for k_6, m=3, n=3).
L	total length of reactor, [m].
N	number of tubes in hybrid reactor, [-].
N_i, N'_i	molar flux of component i inside catalyst particles on shell and tube sides, [mole/m^2/s].

N_p	number of points at which styrene yields and nitrobenzene conversion are predicted, [-].
n_{NBo}	feed molar flowrates of nitrobenzene on tube side [mole/s].
n_i, n'_i	molar flow rate of component i on shell and tube sides, [mole/s].
J_i	molar flux of component i, [mole/m^2/s].
p_i, p'_i	partial pressure of component i on shell and tube sides, [bar].
P, P'	total pressure on shell side and tube side, [bar].
P_f, P'_f	feed pressure on shell side and tube side, [bar].
Q	heat transferred from tube side to shell side, [W/m].
Q_o	pre-exponential constant of hydrogen membrane, [mole/m/s/bar$^{0.5}$].
r_j	rate of reaction j on shell side, [mole/kg cat/s].
r'	rate of hydrogenation reaction on tube side, [mole/kg cat/s].
r_1, r_2	inner and outer radii of hydrogenation tube, [m].
r_3-r_2	thickness of palladium membrane, [m].
T, T'	temperature on shell and tube sides, [K].
T_s, T_s'	temperature at the surface of catalyst pellet on shell and tube sides, [K].
X_{NB}	conversion of nitrobenzene on tube side, [-].
$\tilde{X}_{NB}$	reference conversion of nitrobenzene, i.e. predictions by heterogeneous reactor model with dusty gas diffusion for non-isothermal catalyst pellets at designated distances along reactor, [-].
x_i, x'_i	mole fraction inside catalyst pellet on shell and tube sides, [-].
x_{is}, x'_{is}	mole fraction at the surface of catalyst pellet on shell and tube sides, [-].
Y_{ST}	yield of styrene, [-].
$\tilde{Y}_{ST}$	reference yield of styrene, i.e. predictions by heterogeneous reactor model with dusty gas diffusion for non-isothermal catalyst pellets at designated distances along reactor, [-].

y, y'	radial coordinate inside catalyst pellet on shell and tube sides, [-].
z	axial coordinate along reactor, [m].
$\left[\Delta H(T)\right]_j$	heat of reaction j at temperature T on shell side, [J/mole].
$\left[\Delta H'(T')\right]$	heat of hydrogenation reaction at temperature T' on tube side, [J/mole].
ω, ω'	dimensionless radial distance inside catalyst pellets on shell and tube sides, [-]
ρ_s, ρ'_s	catalyst density on shell and tube sides, [kg/m^3].
σ_{ij}	stoichiometric coefficient of reactant i in reaction j, [-].
δ_{H_2}	thickness of hydrogen permeation membrane, [m].
η	effectiveness factor, [-].

References:

Abashar, M. E., Elnashaie, S. S., 1993. Mathematical modelling of diffusion-reaction, and solution algorithm for complex reaction networks in porous catalyst pellets—steam reforming of natural gas, Mathematical and Computer Modelling 18(7), 85-100.

Abo-Ghander, N. S., Grace, J. R., Elnashaie, S. S. E. H., Lim, C. J., 2008. Modeling of a novel membrane reactor to integrate dehydrogenation of ethylbenzene to styrene with hydrogenation of nitrobenzene to aniline, Chemical Engineering Science 63(7), 1817-1826.

Abo-Ghander, N. S., Logist, F., Grace, J. R., Van Impe, J. F. M., Elnashaie, S. S. E. H., Lim, C. J., 2010a. Optimal design of an autothermal membrane reactor coupling the dehydrogenation of ethylbenzene to styrene with the hydrogenation of nitrobenzene to aniline, Chemical Engineering Science 65(10), 3113-3127.

Abo-Ghander, N. S., Logist, F., Grace, J. R., Van Impe, J. F. M., Elnashaie, S. S. E. H., Lim, C. J., 2010b. Feasibility of coupling dehydrogenation of ethylbenzene with hydrogenation of nitrobenzene in an autothermal catalytic membrane reactor: modeling study, Proceedings of the 9th International Symposium on Dynamics and Control of Process Systems, 365.

Amon, B., Redlingshöfer, H., Klemm, E., Dieterich, E., Emig, G., 1999. Kinetic investigations of the deactivation by coking of a noble metal catalyst in the catalytic hydrogenation of nitrobenzene using a catalytic wall reactor, Chemical Engineering and Processing 38(4-6), 395-404.

Abdalla B. K., Al-Khowaiter S. H., Elshishini S. S., Elnashaie S. S. E. H., October 12 - 17, 1997. Maximization of styrene yield from the catalytic dehydrogenation of ethylbenzene in fixed and fluidized bed configurations with and without selective membranes, 15th World Petroleum Congress, Beijing, China .

Balasubramanian, B., Lopez Ortiz, A., Kaytakoglu, S., Harrison, D. P., 1999. Hydrogen from methane in a single-step process, Chemical Engineering Science 54(15-16), 3543-3552.

Beuscher, U., H. Gooding, C., 1999. The influence of the porous support layer of composite membranes on the separation of binary gas mixtures, Journal of Membrane Science 152(1), 99-116.

Chen, Z., Elnashaie, S. S. E. H., 2005. Autothermal CFB Membrane Reformer for Hydrogen Production from Heptane, Chemical Engineering Research and Design 83(7), 893-899.

Chen, Z., Prasad, P., Yan, Y., Elnashaie, S., 2003. Simulation for steam reforming of natural gas with oxygen input in a novel membrane reformer, Fuel Processing Technology 83(1-3), 235-252.

Elnashaie, S. S. E. H., Abashar, M. E. E., 1993. Steam reforming and methanation effectiveness factors using the dusty gas model under industrial conditions, Chemical Engineering and Processing 32(3), 177-189.

Elnashaie, S. S. E. H., Alhabdan, F. M., 1989. A computer software package for the simulation and optimization of an industrial ammonia converter based on a rigorous heterogeneous model, Mathematical and Computer Modelling 12(12), 1589-1600.

Elnashaie, S. S. E. H., Moustafa, T., Alsoudani, T., Elshishini, S. S., 2000. Modeling and basic characteristics of novel integrated dehydrogenation — hydrogenation membrane catalytic reactors, Computers & Chemical Engineering 24(2-7), 1293-1300.

Elnashaie, S. S. E. H., Soliman, M. A., Abashar, M. E., Almuhana, S., 1992. Mathematical modelling of diffusion and reaction for gas-solid catalytic systems with complex reaction networks. Negative effectiveness factors, Mathematical and Computer Modelling 16(12), 41-53.

Elnashaie, S. S. E. H., Abdalla, B. K., Hughes, R., 1993. Simulation of the industrial fixed bed catalytic reactor for the dehydrogenation of ethylbenzene to styrene: heterogeneous dusty gas model, Industrial & Engineering Chemistry Research 32(11), 2537-2541.

Froment G. F., Bischoff K. B. , 1990. Chemical Reactor Analysis and Design. USA: John Wiley & Sons, Inc.

Hermann, C., Quicker, P., Dittmeyer, R., 1997. Mathematical simulation of catalytic dehydrogenation of ethylbenzene to styrene in a composite palladium membrane reactor, Journal of Membrane Science 136(1-2), 161-172.

Itoh, N., Xu, W. C., Hara, S., Kakehida, K., Kaneko, Y., Igarashi, A., 2003. Effects of hydrogen removal on the catalytic reforming of n-hexane in a palladium membrane reactor, Industrial & Engineering Chemistry Research 42(25), 6576-6581.

Itoh, N., Wu, T., 1997. An adiabatic type of palladium membrane reactor for coupling endothermic and exothermic reactions, Journal of Membrane Science 124(2), 213-222.

Krishna, R., 1990. Multicomponent surface diffusion of adsorbed species: a description based on the generalized Maxwell—Stefan equations, Chemical Engineering Science 45(7), 1779-1791.

Krishna, R., Wesselingh, J. A., 1997. The Maxwell-Stefan approach to mass transfer, Chemical Engineering Science 52(6), 861-911.

Logist, F., Van Erdeghem, P. M. M., Van Impe, J. F., 2009. Efficient deterministic multiple objective optimal control of (bio)chemical processes, Chemical Engineering Science 64(11), 2527-2538.

Moustafa, T. M., Elnashaie, S. S. E. H., 2000. Simultaneous production of styrene and cyclohexane in an integrated membrane reactor, Journal of Membrane Science 178(1-2), 171-184.

Rakib, M. A., Grace, J. R., Elnashaie, S. S. E. H., Lim, C. J., Bolkan, Y. G., 2008. Kinetic simulation of a compact reactor system for hydrogen production by steam reforming of higher hydrocarbons, The Canadian Journal of Chemical Engineering 86(3), 403-412.

Elnashaie S.S.E.H., Elshishini S.S., 1993. Modelling, Simulation and Optimization of Industrial Fixed Bed Catalytic Reactors. Amesterdam: Gordon and Breach Science Publisher.

Soliman, M. A., El-Nashaie, S. S. E. H., Al-Ubaid, A. S., Adris, A., 1988. Simulation of steam reformers for methane, Chemical Engineering Science 43(8), 1801-1806.

Tiemersma, T. P., Patil, C. S., Sint Annaland, M. v., Kuipers, J. A. M., 2006. Modelling of packed bed membrane reactors for autothermal production of ultrapure hydrogen, Chemical Engineering Science 61(5), 1602-1616.

Uemiya, S., Sato, N., Ando, H., Matsuda, T., Kikuchi, E., 1990. Steam reforming of methane in a hydrogen-permeable membrane reactor, Applied Catalysis 67(1), 223-230.

Veldsink, J. W., Versteeg, G. F., Van Swaaij, W. P. M., Van Damme, R. M. J., 1995. The use of the dusty-gas model for the description of mass transport with chemical reaction in porous media, The Chemical Engineering Journal and the Biochemical Engineering Journal 57(2), 115-125.

Wang, Y., Xu, Y., Xiang, H., Li, Y., Zhang, B., 2001. Modeling of Catalyst Pellets for Fischer-Tropsch Synthesis, Industrial & Engineering Chemistry Research 40(20), 4324-4335.

Journal homepage: http://www.sciencedirect.com/science/journal/00981354
Original file available at: http://dx.doi.org/10.1016/j.compchemeng.2011.10.007

Table 1: Stoichiometric equations, heats of reactions and reaction rate expressions for reactions considered.

Chemical Reaction	Heat of Reaction	Kinetic Equation	Reference
	Dehydrogenation Side [a]		
$C_6H_5CH_2CH_3 \Leftrightarrow C_6H_5CHCH_2 + H_2$	$\Delta H_{298} = 117.6 \frac{kJ}{mole}$	$r_1 = k_1\left(p_{EB} - p_{ST}\frac{p_{H_2}}{K_A}\right)$	Elnashaie, et al, 1993
$C_6H_5CH_2CH_3 \rightarrow C_6H_6 + C_2H_4$	$\Delta H_{298} = 105.4 \frac{kJ}{mole}$	$r_2 = k_2\, p_{EB}$	Elnashaie, et al, 1993
$C_6H_5CH_2CH_3 + H_2 \rightarrow C_6H_5CH_3 + CH_4$	$\Delta H_{298} = -54.6 \frac{kJ}{mole}$	$r_3 = k_3\, p_{EB}\, p_{H_2}$	Elnashaie, et al, 1993
$2H_2O + C_2H_4 \rightarrow 2CO + 4H_2$	$\Delta H_{298} = 210.2 \frac{kJ}{mole}$	$r_4 = k_4\, p_{H_2O}\, p_{C_2H_4}^{1/2}$	Elnashaie, et al, 1993
$H_2O + CH_4 \rightarrow CO + 3H_2$	$\Delta H_{298} = 206.1 \frac{kJ}{mole}$	$r_5 = k_5\, p_{H_2O}\, p_{CH_4}$	Elnashaie, et al, 1993
$H_2O + CO \rightarrow CO_2 + H_2$	$\Delta H_{298} = -41.2 \frac{kJ}{mole}$	$r_6 = k_6\left(\frac{P}{T^3}\right) p_{H_2O}\, p_{CO}$	Elnashaie, et al, 1993
	Hydrogenation Side [b]		
$C_6H_5NO_2 + 3H_2 \rightarrow C_6H_5NH_2 + 2H_2O$	$\Delta H_{298} = -443.0 \frac{kJ}{mole}$	$r' = \frac{k' K_{NB} K_{H_2}\, p'_{NB}\sqrt{p'_{H_2}}}{\left(1 + K_{NB}\, p'_{NB} + K_{H_2}\sqrt{p'_{H_2}}\right)^2}$	Amon, et al, 1999

[a] partial pressure in (bars)
[b] partial pressure in (kPa)

Table 2: Frequency factors and activation energies for reactions considered.

Reaction[a]	k_{io}[b]	E_i (kJ/kmol)	Reference
1[b]	8.32×10^{3}	0.909×10^{5}	Elnashaie, et al, 1993b
2	4.23×10^{9}	2.080×10^{5}	
3	6.13×10^{3}	0.915×10^{5}	
4	3.95×10^{3}	1.040×10^{5}	
5	1.42×10^{2}	0.657×10^{5}	
6	5.80×10^{12}	0.736×10^{5}	
7[c]	1.86×10^{-4}	10.0×10^{3}	Amon, et al, 1999

[a] Reactions are numbered 1 to 7 in the same order as they are listed in Table 1.

[b] $k_i = \frac{10}{36} k_{io} \exp(-\frac{E_i}{RT})$, where k_{io} is the pre-exponential factor for $1 \le i \le 6$

$k_i = 10^3 k_{io} \exp(-\frac{E_i}{RT})$, for $i = 7$.

The equilibrium constant is calculated by: $K_A = \exp(\frac{-\Delta F}{RT})$, where: $\Delta F = a + bT + cT^2$,

$a=122725.16, b=-126.27/K, c=-2.194\times10^{-3}/K^2$

[d] $K_{NB} = 1.51\times10^{-2}$ kPa, $K_{H_2} = 0.14\,kPa^{-0.5}$

Table 3: Model equations for coupled catalytic membrane reactor.

Balance Equations	Mathematical Expressions	Equation
	Dehydrogenation Side	
Mole	$\frac{dn_i}{dz}=\sum_{j=1}^{6}\sigma_{ij}\left(3\int_0^{1.0} r_j\omega^2 d\omega\right)(1-\varepsilon)A_{cs}\rho_s-2\pi r_3 Na_i J_i$	**(8)**
Energy	$\frac{dT}{dz}=\frac{\sum_{j=1}^{6}\left(3\int_0^{1.0}\left[-\Delta H(T)\right]_j r_j\omega^2 d\omega\right)(1-\varepsilon)A_{cs}\rho_s+Q}{\sum_{i=1}^{10} n_i Cp_i}$	**(9)**
Pressure	$\frac{dP}{dz}=-\frac{G}{\rho_g g_c D_p}\left(\frac{1-\varepsilon}{\varepsilon^3}\right)\left[\frac{150(1-\varepsilon)\mu_g}{D_p}+1.75G\right]$	**(10)**
	Hydrogenation Side	
Mole	$\frac{dn'_i}{dz}=\sigma_i\left(3\int_0^{1.0} r'\omega'^2 d\omega'\right)(1-\varepsilon')A'_{cs}\rho'_s+2\pi r_3 a_i J_i$	**(11)**
Energy	$\frac{dT'}{dz}=\frac{(2\pi r_3)\sum_{i=1}^{i} a_i J_i\int_{T'}^{T} Cp_i dT+\left(3\int_0^{1.0}\left[-\Delta H'(T')\right]r'\omega'^2 d\omega\right)(1-\varepsilon')A'_{cs}\rho'_s-Q}{\sum_{i=1}^{4} n'_i Cp'_i}$	**(12)**
Pressure	$\frac{dP'}{dz}=-\frac{G'}{\rho'_g g_c D'_p}\left(\frac{1-\varepsilon'}{\varepsilon'^3}\right)\left[\frac{150(1-\varepsilon')\mu'_g}{D'_p}+1.75G'\right]$	**(13)**
	Additional Relations	
Diffusion of Hydrogen across Membrane	$J_{H_2}=\frac{Q_o\exp\left(-\frac{E_{H_2,P}}{RT}\right)}{\delta_{H_2}}\left(\sqrt{P_{H_2}}-\sqrt{P'_{H_2}}\right)$ where: $Q_o=7.29\times10^{-03}$ (mole×m)/(m^2×min×atm$^{0.5}$), $\delta_{H_2}=25\times10^{-6}$ m, $E_{H_2,P}=20.5\times10^3$ J/mole	**(14)**
Heat Transfer across Membrane	$Q=\frac{2\pi r_1(T'-T)}{\left[\frac{1}{h'}+\frac{r_1}{k_{ss}}\ln\left(\frac{r_2}{r_1}\right)+\frac{r_1}{k_{Pd}}\ln\left(\frac{r_3}{r_2}\right)+\frac{r_1}{r_2 h}\right]}$ where: k_{ss}=22.88 W/m/K, k_{Pd}=93.30 W/m/K, $\frac{hD_t}{k_g}=0.813\left(\frac{D_p G}{\mu_g}\right)^{0.9}\exp\left(-\frac{6D_p}{D_t}\right)$ $\frac{h'D'_t}{k'_g}=3.50\left(\frac{D'_p G'}{\mu'_g}\right)^{0.7}\exp\left(-\frac{4.6D'_p}{D'_t}\right)$	**(15)**

Table 4: Base case dimensional and operating parameters for coupled catalytic membrane reactor.

Parameter	Values	Units
Dimensional Variables		
Cross-sectional area-equivalent diameter of dehydrogenation side	1.95	m
Inside diameter of hydrogenation tubes	3.5×10^{-2}	m
Total number of hydrogenation tubes	1500	----
Length of reactor	4.0	m
Operating Conditions of Dehydrogenation Side		
Feed molar flowrate of ethylbenzene	10.242	mole/s
Feed molar flowrate of styrene	0.1861	mole/s
Feed molar flowrate of benzene	0.0306	mole/s
Feed molar flowrate of toluene	0.2444	mole/s
Feed molar flowrate of steam	125.86	mole/s
Feed temperature	880.0	K
Feed pressure	2.5	bar
Catalyst density	2146.3	kg/m^3
Catalyst thermal conductivity	0.3	J/m/s
Pore diameter	4800×10^{-10}	m
Catalyst porosity	0.35	----
Catalyst tortuosity	4.0	----
Bed voidage	0.48	----
Operating Conditions **per tube** on Hydrogenation Side		
Feed molar flowrate of nitrobenzene	0.003	mole/s
Feed molar flowrate of steam	0.008	mole/s
Inlet temperature	900.0	K
Inlet pressure	1.0	bar
Catalyst density	1400	kg/m^3
Catalyst thermal conductivity	0.05	J/m/s
Pore diameter	5000×10^{-10}	m
Catalyst porosity	0.40	----
Catalyst tortuosity	4.0	----
Bed voidage	0.46	----

Table 5: Representative solutions for Pareto frontier. Values shown in bold are constrained limits.

Parameter				Optimal case A	Optimal case B	Optimal case C
Dehydrogenation Side	Feed Molar flowrate of Ethylbenzene (mole/s)			**7.66**	9.36	**11.27**
	Steam-to-Ethylbenzene Ratio			**7.00**	**7.00**	**20.00**
	Feed Temperature on Shell Side (K)			825.41	780.00	820.02
	Feed Pressure on Shell Side (bar)			**4.00**	2.52	**4.00**
Hydrogenation Side (one tube basis)	Feed Molar flowrate of Nitrobenzene (mol/s)			**0.005**	**0.002**	**0.002**
	Steam-to-Nitrobenzene Ratio			**4.00**	**4.00**	**4.00**
	Feed Temperature on Tube Side (K)			825.41	780.00	820.02
	Feed Pressure on Tube Side (bar)			3.62	**1.00**	**1.00**
Dimensional Variables	No. of Hydrogenation Tubes			**2500**	1582	**1000**
	Equivalent-area Diameter of Dehydrogenation Side (m)			**3.00**	2.39	**1.95**
	Diameter of Hydrogenation Tube (m)			0.048	0.035	0.040
	Reactor Length (m)			**4.00**	**4.00**	**4.00**
Yield of Styrene	Homogeneous Modeling			0.975	0.564	0.491
	Heterogeneous Modeling	Fickian Diffusion Model	Isothermal Catalyst Pellets	0.930	0.512	0.426
			Non-isothermal Catalyst Pellets	0.925	0.478	0.386
		Dusty Gas Model	Isothermal Catalyst Pellets	0.942	0.522	0.429
			Non-isothermal Catalyst Pellets	0.894	0.4864	0.3956
Conversion of Nitrobenzene	Homogeneous Modeling			0.211	0.555	0.796
	Heterogeneous Modeling	Fickian Diffusion Model	Isothermal Catalyst Pellets	0.208	0.502	0.713
			Non-isothermal Catalyst Pellets	0.201	0.467	0.6594
		Dusty Gas Model	Isothermal Catalyst Pellets	0.210	0.514	0.727
			Non-isothermal Catalyst Pellets	0.204	0.479	0.681

Table 6: Deviations of the predictions inside the coupled reactor from the non-isothermal dusty gas heterogeneous reactor model.

Reactor Models		Yield of Styrene		Conversion of Nitrobenzene	
		Root mean square deviation	Absolute mean deviation	Root mean square deviation	Absolute mean deviation
Operating Condition in Table 4	Homogeneous	0.113	0.109	0.0848	0.0801
	Heterogeneous, Fickian, Isothermal	0.0294	0.0286	0.0167	0.0155
	Heterogeneous, Fickian, Non-isothermal	0.0214	0.0211	0.0312	0.0284
	Heterogeneous, Dusty Gas , Isothermal	0.0335	0.0321	0.0297	0.0281
Case A	Homogeneous	0.111	0.110	0.0193	0.0187
	Heterogeneous, Fickian, Isothermal	0.0442	0.0436	0.0073	0.0071
	Heterogeneous, Fickian, Non-isothermal	0.0108	0.0095	0.0027	0.0026
	Heterogeneous, Dusty Gas , Isothermal	0.0557	0.0055	0.0094	0.0092
Case B	Homogeneous	0.0521	0.0485	0.0530	0.0499
	Heterogeneous, Fickian, Isothermal	0.0188	0.0178	0.0160	0.0147
	Heterogeneous, Fickian, Non-isothermal	0.0087	0.0086	0.0101	0.0096
	Heterogeneous, Dusty Gas , Isothermal	0.0243	0.0225	0.0250	0.0234
Case C	Homogeneous	0.0717	0.0674	0.0990	0.0934
	Heterogeneous, Fickian, Isothermal	0.0225	0.0211	0.0247	0.0225
	Heterogeneous, Fickian, Non-isothermal	0.0092	0.0090	0.0177	0.0164
	Heterogeneous, Dusty Gas , Isothermal	0.0242	0.0224	0.0380	0.0357

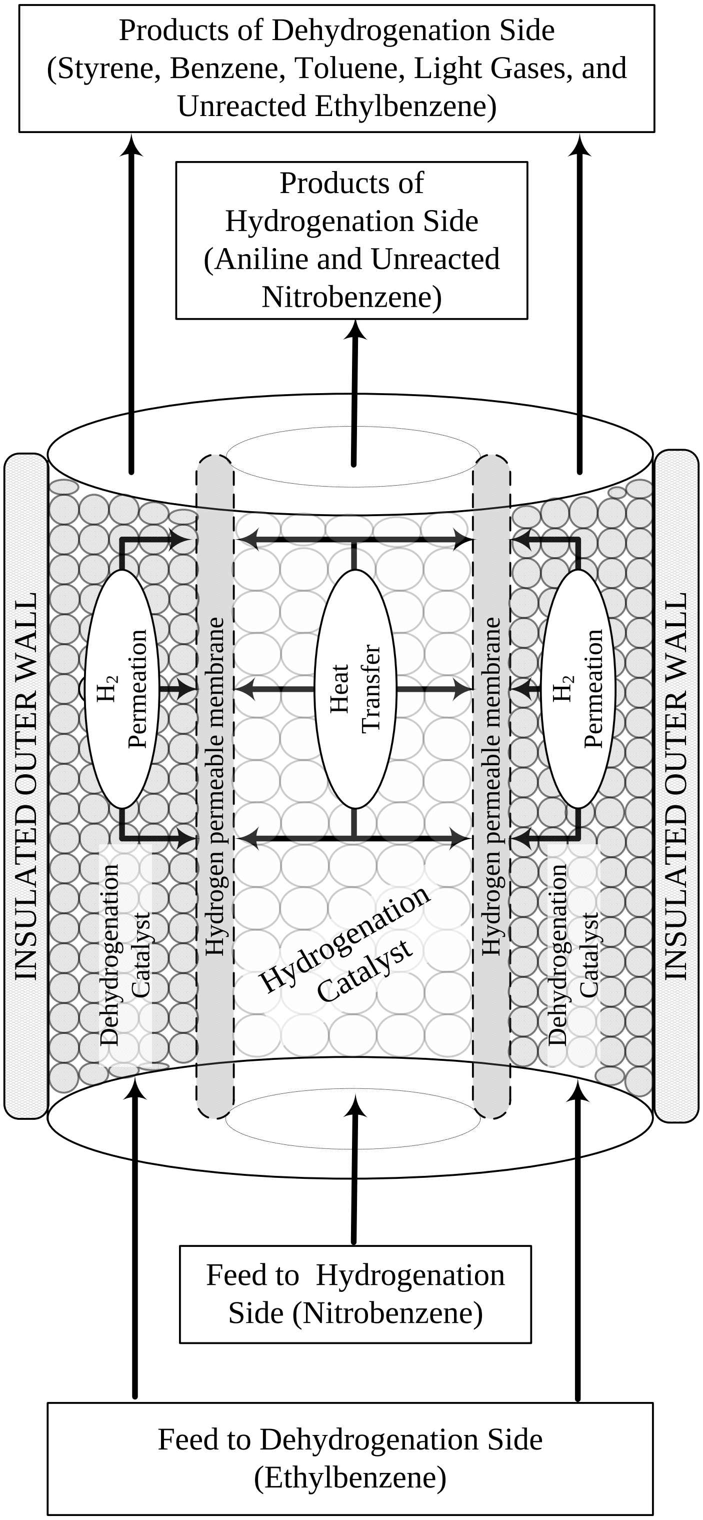

Figure 1: Schematic of integrated membrane fixed bed reactor with cocurrent flow.

Journal homepage: http://www.sciencedirect.com/science/journal/00981354
Original file available at: http://dx.doi.org/10.1016/j.compchemeng.2011.10.007

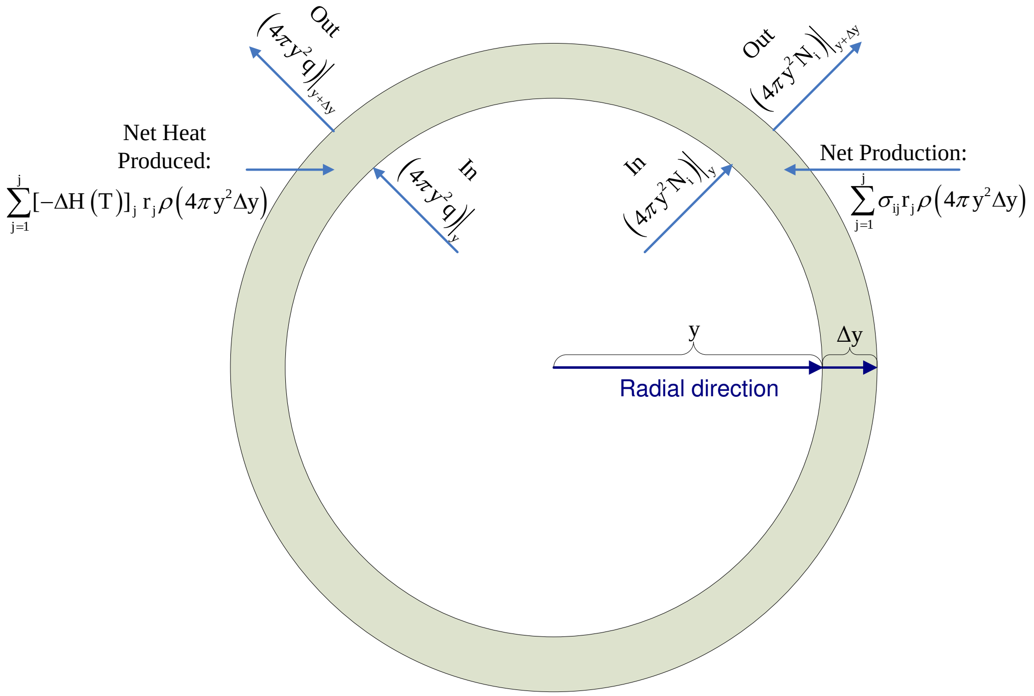

Figure 2: Molar and heat fluxes across a small shell inside a catalyst pellet.

Journal homepage: http://www.sciencedirect.com/science/journal/00981354
Original file available at: http://dx.doi.org/10.1016/j.compchemeng.2011.10.007

Postprint version of paper published in Computers & Chemical Engineering 2012, vol. 38, pages 11-23.
The content is identical to the published paper, but without the final typesetting by the publisher.

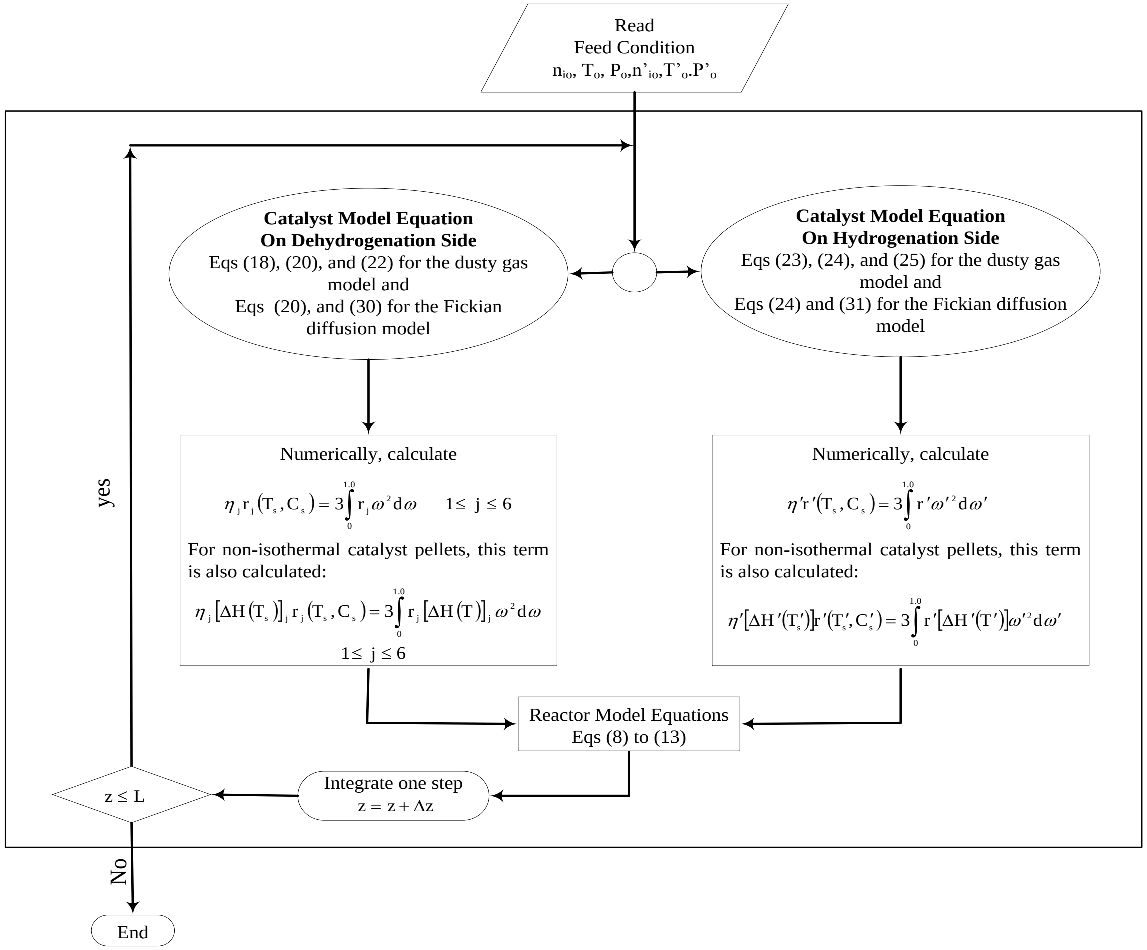

Figure 3: Computational sequence coupling dusty gas model equations with reactor model equations

Journal homepage: http://www.sciencedirect.com/science/journal/00981354
Original file available at: http://dx.doi.org/10.1016/j.compchemeng.2011.10.007

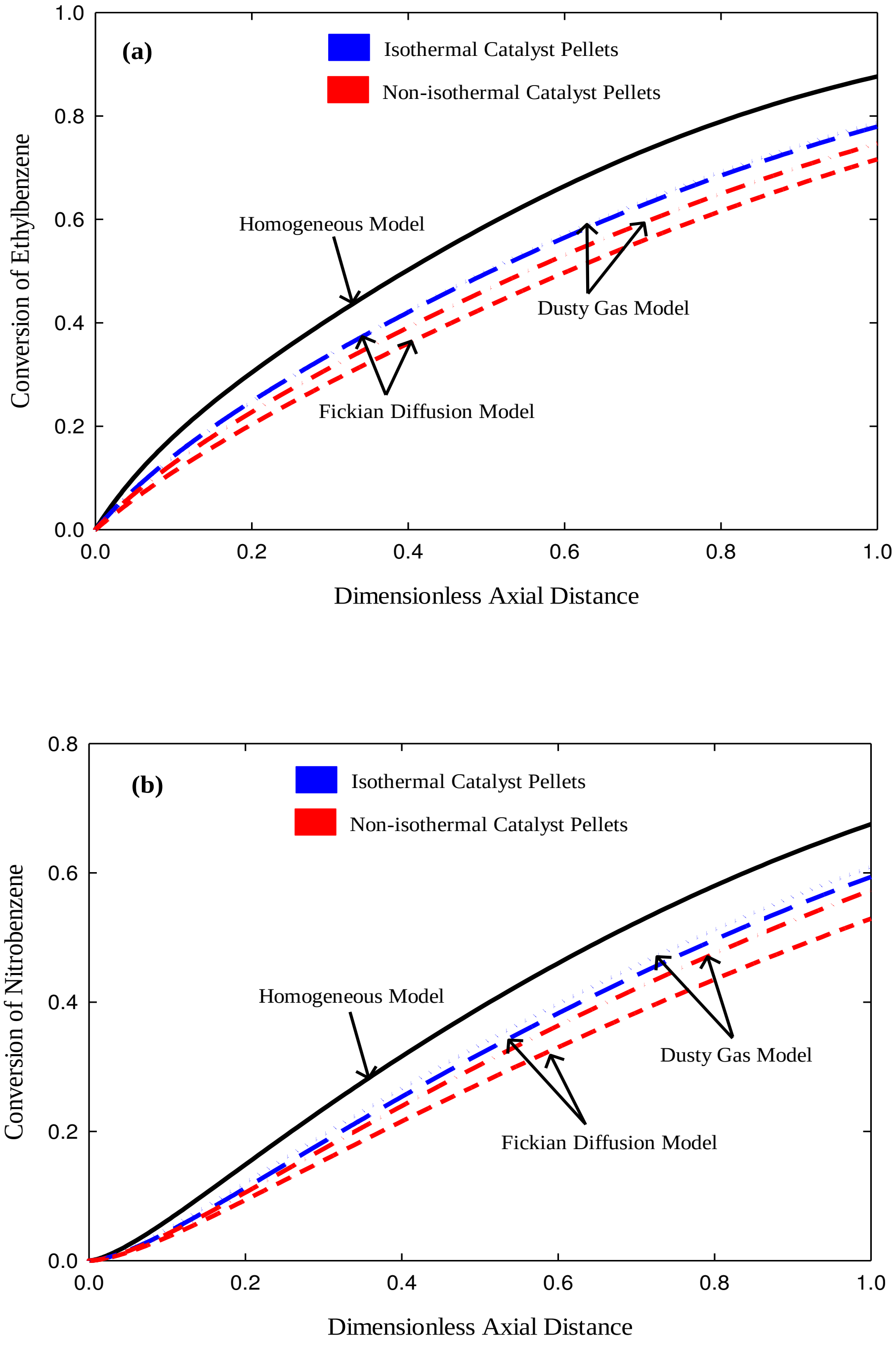

Figure 4: Conversion of (a) ethylbenzene on dehydrogenation side, and (b) nitrobenzene on hydrogenation side for base case operating conditions in Table 4.

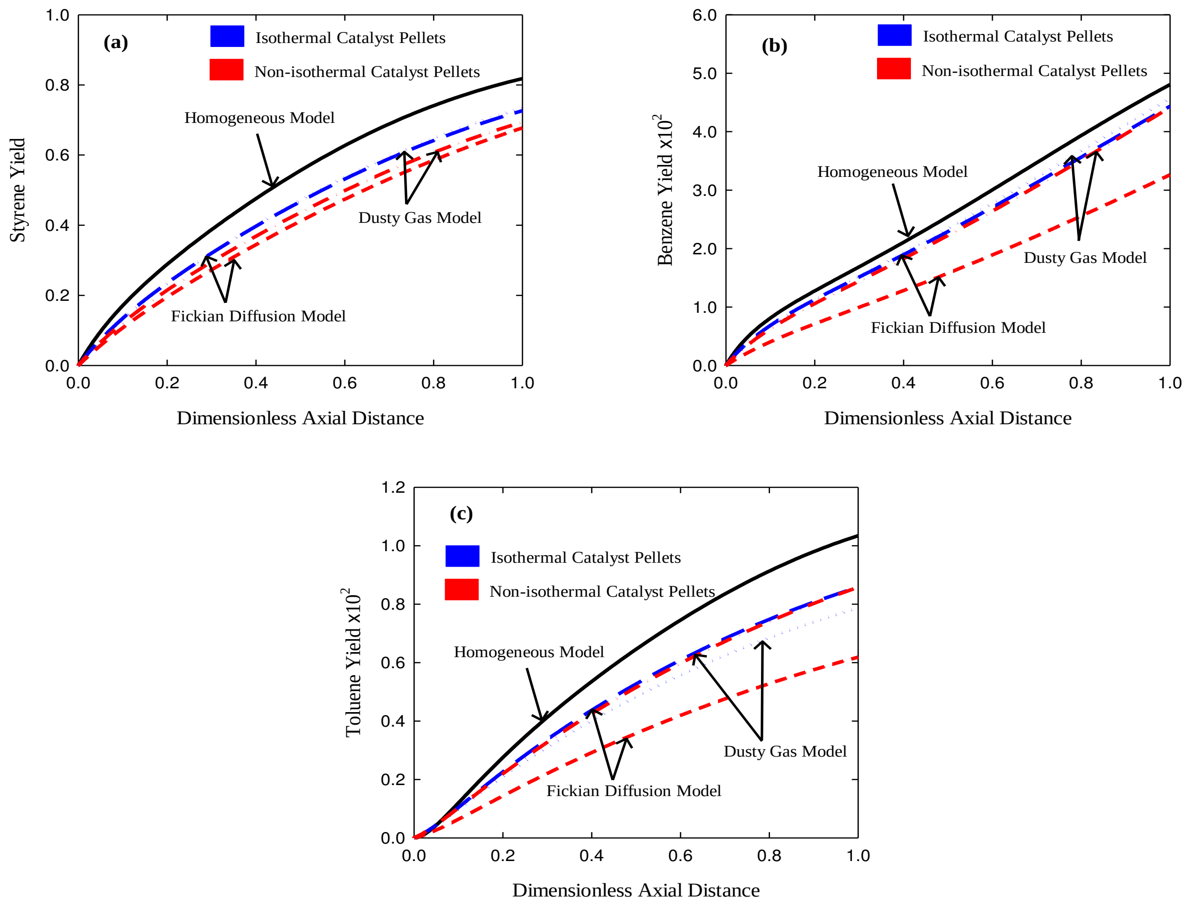

Figure 5: Yield of (a) Styrene, (b) Benzene, and (c) Toluene along dehydrogenation side for base case operating conditions in Table 4.

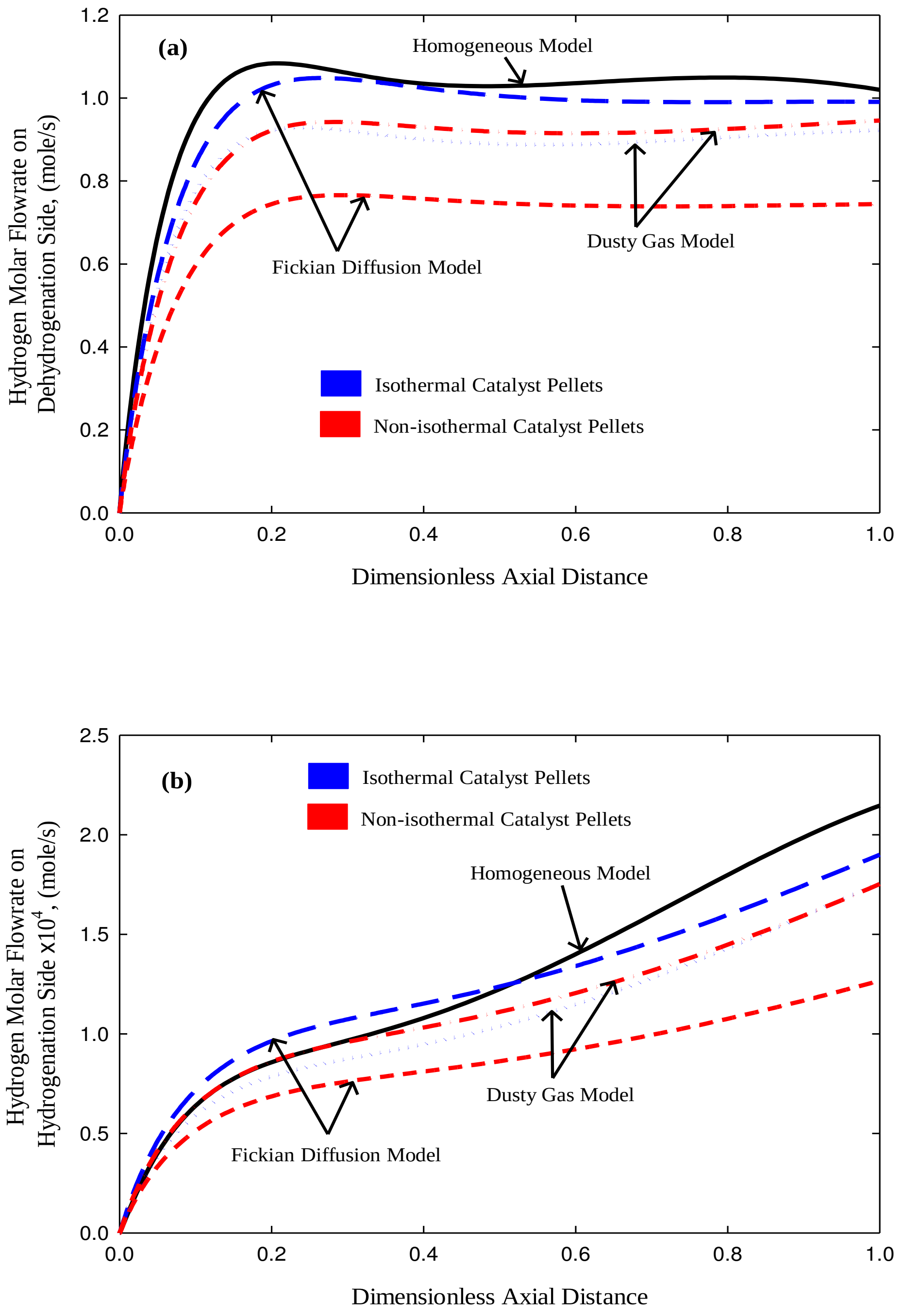

Figure 6: Hydrogen molar flowrate variation along reactor for base case operating conditions in Table 4 on: (a) dehydrogenation side, (b) hydrogenation side.

Postprint version of paper published in Computers & Chemical Engineering 2012, vol. 38, pages 11-23.
The content is identical to the published paper, but without the final typesetting by the publisher.

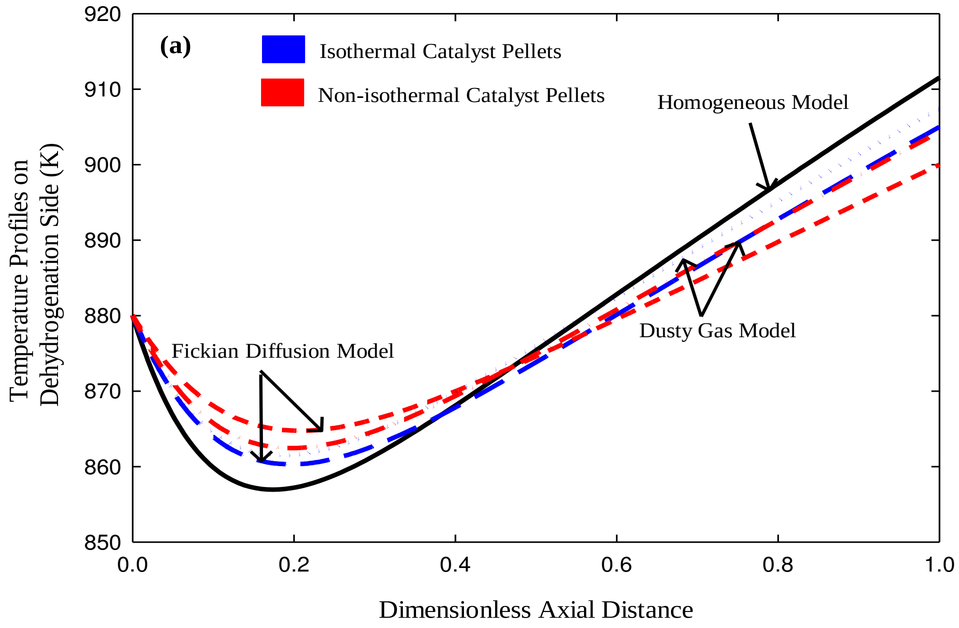

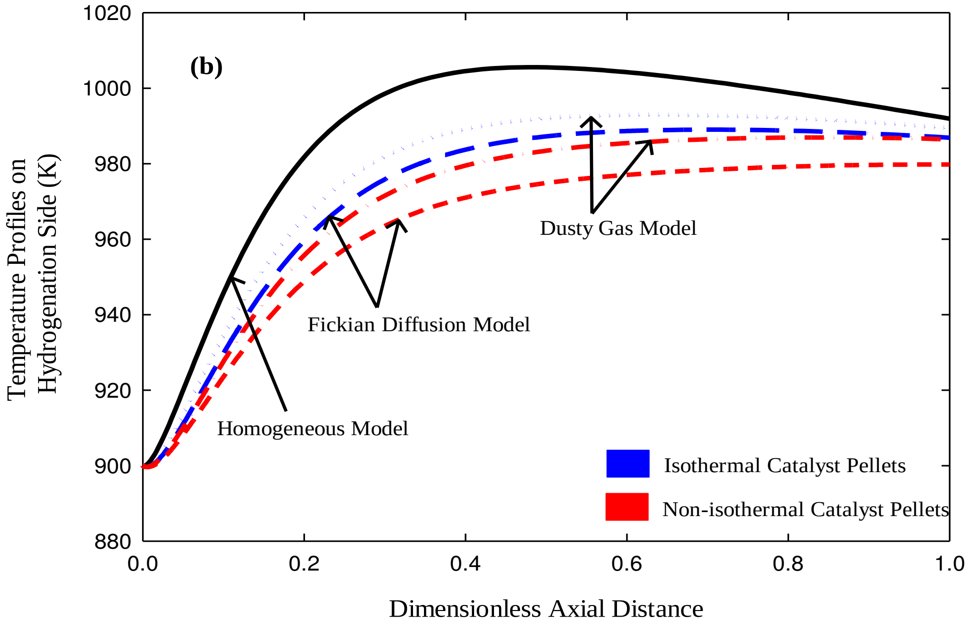

Figure 7: Temperature profiles along the reactor for base case operating conditions in Table 4 on: (a) dehydrogenation side, and (b) hydrogenation side.

Journal homepage: http://www.sciencedirect.com/science/journal/00981354
Original file available at: http://dx.doi.org/10.1016/j.compchemeng.2011.10.007